A Narrow-Passband and Frequency-Tunable Microwave Photonic Filter Based on Phase-Modulation to Intensity-Modulation Conversion Using a Phase-Shifted Fiber Bragg Grating

Wangzhe Li, *Student Member, IEEE*, Ming Li, *Member, IEEE*, and Jianping Yao, *Fellow, IEEE*

***Abstract*—A novel approach to implementing a narrow-passband and frequency-tunable microwave photonic filter (MPF) based on phase-modulation to intensity-modulation conversion in a phase-shifted fiber Bragg grating (PS-FBG) is proposed and experimentally demonstrated. In the proposed MPF, a phase-modulated signal is sent to a PS-FBG. If one of the sidebands falls in the notch of the PS-FBG, the phase-modulated signal is converted to an intensity-modulated signal. Due to the ultra-narrow notch of the PS-FBG, a microwave filter with an ultra-narrow passband is realized. The tunability of the microwave filter is achieved by tuning the wavelength of the optical carrier. A theoretical analysis is performed in which the value of the phase shift and the location of the phase shift in the PS-FBG on the frequency response of the MPF are studied. Two PS-FBGs with different reflection bandwidths and different phase-shift values introduced at the center of the gratings are fabricated and incorporated into the proposed MPF. For the two PS-FBGs, the 3-dB bandwidths are 120 and 60 MHz and the tunable ranges are 5.5 and 15 GHz.**

***Index Terms*—Fiber Bragg grating (FBG), microwave photonic filter (MPF), microwave photonics, phase-modulation to intensity-modulation (PM–IM) conversion, phase modulator.**

I. Introduction

MICROWAVE filters implemented in the optical domain have been intensively studied in the past few years. Compared with microwave filters implemented in the electrical domain, microwave photonic filters (MPFs) exhibit unique properties such as high frequency, large tunability, light weight, and immunity to electromagnetic interference [1]–[3], which can find numerous applications, such as in modern radar and warfare systems. An MPF usually has a delay-line structure with a finite impulse response (FIR). The bandpass selectivity of an MPF is mainly determined by the number of taps [4]. To avoid optical interference, the multiple taps are usually realized by using a multiwavelength light source, such as a laser array, a broadband spectrum-sliced source, or an optical comb source [5]–[9]. To improve the selectivity, the number of the taps should be large, but at the cost of increased complexity. An MPF can also be implemented with an infinite impulse response (IIR). Compared with an FIR filter, an IIR filter usually has a simpler structure and better selectivity [10]–[13]. However, due to the use of resonators [12] or feedback loops [13] in an IIR filter, the stability is poor and the tunability is limited. To implement an MPF with large tunability, stimulated Brillouin scattering (SBS) can be employed in which the Brillouin gain is used to selectively amplify the sideband of the single-sideband modulated light wave [14]. However, a double-sideband with suppressed carrier modulation and single-sideband modulation are needed, which significantly increase the complexity and cost of the system. In [15], such a complicated modulation technique is replaced by using an optical filter, and an SBS-based tunable true time-delay line has been proposed to implement a dynamically reconfigurable MPF. The time delay can be tuned by changing the SBS pump power. The major limitation of the approach is that multiple modulators are employed, making the system complicated. An MPF can also be achieved based on phase-modulation to intensity-modulation (PM–IM) conversion. By selecting the optical carrier and one sideband of a phase-modulated light wave using two uniform fiber Bragg gratings (FBGs) [16], a phase-modulated signal is converted to an intensity-modulated signal. The major limitation of the approach is that the passband is wide, which is determined by the bandwidth of the uniform FBG used to select the sideband. The use of a ring resonator to filter out one sideband of a phase-modulated light wave can also achieve an MPF with potentially large tunability [17]. Since the bandwidth of the ring resonator is wide, the width of the passband is wide, in the range of several gigahertz. For many applications, an MPF with a narrow passband is needed.

In this paper, we propose and experimentally demonstrate a narrow-passband and frequency-tunable MPF based on PM–IM conversion employing a phase-shifted fiber Bragg grating (PS-FBG) that serves as a reflection filter with an ultra-narrow notch in the reflection band. In the proposed MPF, a microwave signal

Manuscript received July 02, 2011; revised January 28, 2012; accepted February 02, 2012. Date of publication March 12, 2012; date of current version April 27, 2012. This work was supported by the Natural Sciences and Engineering Research Council of Canada (NSERC).

The authors are with the Microwave Photonics Research Laboratory, School of Electrical Engineering and Computer Science, University of Ottawa, Ottawa, ON, Canada K1N 6N5 (e-mail: jpyao@site.uottawa.ca).

Color versions of one or more of the figures in this paper are available online at http://ieeexplore.ieee.org.

Digital Object Identifier 10.1109/TMTT.2012.2187678

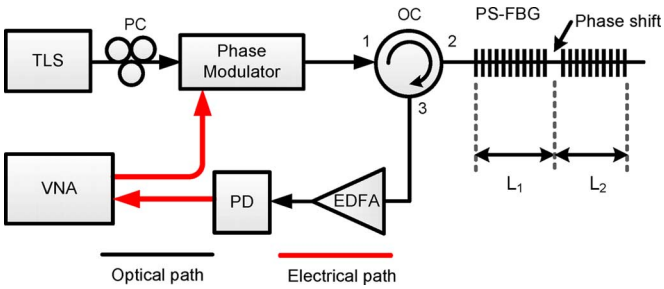

Fig. 1. Schematic of the proposed MPF. L_1 and L_2 are, respectively, the lengths of the left and right sub-FBGs separated by the phase shift.

is modulated on an optical carrier at a phase modulator. The phase-modulated signal is then sent to the PS-FBG. When one of the first-order sidebands falls in the notch of the PS-FBG, the magnitude and phase of the sideband are modified, and the magnitude and phase relationship for the phase-modulated signal is no longer maintained; thus the phase-modulated signal is converted to an intensity-modulated signal, and the detection of the intensity-modulated signal at a photodetector (PD) would lead to the generation of an electrical signal. Due to the ultra-narrow notch of the PS-FBG, an MPF with an ultra-narrow passband is implemented. The tunability of the MPF can be easily achieved by tuning the wavelength of the optical carrier, and the frequency tuning range can be as wide as tens of gigahertz, which is determined by the reflection bandwidth of the PS-FBG and the notch location within the reflection band. A theoretical analysis is performed in which the value of the phase shift and the location of the phase shift in the PS-FBG on the frequency response of the MPF are studied. Two PS-FBGs with different reflection bandwidths and different phase-shift values introduced at the center of the gratings are fabricated and are incorporated into the proposed MPF. For the two PS-FBGs, the 3-dB bandwidths are 120 and 60 MHz and the tunable ranges are 5.5 and 15 GHz. To the best of our knowledge, the 15-GHz frequency tuning range is the widest frequency-tunable range ever demonstrated for a single bandpass MPF.

II. Principle of Operation

The configuration of the proposed MPF is shown in Fig. 1. It consists of a tunable laser source (TLS), a polarization controller (PC), a phase modulator, an optical circulator (OC), a PS-FBG, an erbium-doped fiber amplifier (EDFA), and a PD. In the proposed MPF, a continuous wave (CW) light wave with a tunable angular frequency of ω_o from the TLS is sent to the phase modulator via the PC. The polarization state of the light wave to the phase modulator is adjusted by the PC to minimize the polarization-dependent loss. The phase modulator is driven by a sinusoidal microwave signal with a tunable angular frequency ω_e generated by a vector network analyzer (VNA).

If the phase-modulated signal is applied directly to the PD, no signal would be detected, except a dc since the beating between the optical carrier and the upper sideband will cancel completely the beating between the optical carrier and the lower sideband, due to the fact that the two beat signals are out of phase. However, it is well known that a phase-modulated signal can be converted to an intensity-modulated signal if the magnitude or phase relationship among the two sidebands and the

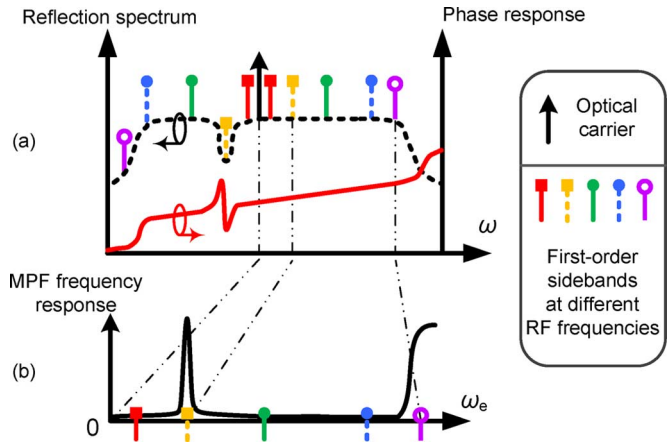

Fig. 2. Illustration of the operation of the MPF. (a) Reflection spectrum (dashed line) and phase response (solid line) of the PS-FBG. (b) Frequency response of the MPF.

optical carrier is changed, and such PM–IM conversion has a transfer function corresponding to a bandpass filter [18]. It is also well known for a uniform FBG, if a phase shift is introduced to the FBG, an ultra-narrow notch with a phase jump in the notch would be generated in the reflection band [19]. Thus, in our system, the phase-modulated light wave is injected into the PS-FBG that is employed to modify the magnitude and the phase of either the upper or the lower sideband falling in the ultra-narrow notch of the PS-FBG, to achieve PM–IM conversion, leading to the implementation of an ultra-narrow passband, as shown in Fig. 2.

Note that if ω_e is too large such that one sideband of the phase-modulated light wave is located outside the reflection spectrum, as shown in Fig. 2(a), PM–IM conversion would also happen and another passband at much higher frequencies would appear, as shown in Fig. 2(b). Practically, the reflection bandwidth of the PS-FBG could be large enough such that the second passband would be beyond the bandwidth of the PD. Thus, the proposed MPF will have a single bandpass. The central frequency of the achieved bandpass filter is equal to the frequency difference between the frequency of the optical carrier and that of the notch. Therefore, by simply tuning the wavelength of the optical carrier, the center frequency of the MPF can be tuned. The tuning range is determined by the total reflection bandwidth of the PS-FBG and the location of the notch within the reflection band.

Mathematically, the electrical field $E_{\mathrm{PM}}(t)$ at the output of the phase modulator can be expressed as [20]

$$\begin{aligned} E_{\mathrm{PM}}(t) &= E_o \exp\left[j\omega_o t + j\beta\cos\left(\omega_e t + \varphi_e\right)\right] \\ &= E_o \sum_{n=-\infty}^{\infty} i^n J_n(\beta) \exp\left\{j\left[\omega_o t + n\left(\omega_e t + \varphi_e\right)\right]\right\} \\ &\approx E_o J_0(\beta)\exp\left(j\omega_o t\right) \\ &\quad + E_o J_1(\beta)\exp\left[j\left(\omega_o t + \omega_e t + \varphi_e + \frac{\pi}{2}\right)\right] \\ &\quad - E_o J_1(\beta)\exp\left[j\left(\omega_o t - \omega_e t - \varphi_e - \frac{\pi}{2}\right)\right] \end{aligned} \quad (1)$$

where E_o is the electrical amplitude of the incident light wave, $J_n(\cdot)$ is the nth-order Bessel function of the first kind, φ_e is the initial phase of the microwave drive signal applied to the phase

modulator, and $\beta = \pi V/V_\pi$ is the phase modulation index, where V is the amplitude of the signal applied to the phase modulator, and V_π is the half-wave voltage of the phase modulator. The value of the phase modulation index is set small so that the power of the second-order and higher order sidebands is much smaller than that of the carrier and the first-order sidebands. Therefore, only the optical carrier and the two first-order sidebands are considered.

Since the amplitude and the phase of the optical carrier and the sidebands will be modified by the PS-FBG, in the following, we will give the amplitude response and the phase response of the PS-FBG first. The PS-FBG can be described by a 2×2 matrix $\boldsymbol{F}$ through

$$\boldsymbol{F} = {}^{2}F \cdot {}^{\mathrm{PS}}F \cdot {}^{1}F \tag{2}$$

where ${}^{\mathrm{PS}}F$ is a 2×2 diagonal phase-shifted matrix with elements $\exp(\mp j\varphi_{\mathrm{PS}}/2)$, where φ_{PS} is the phase shift; the ${}^{i}F$ is a matrix describing each sub-FBG at each side of the phase shift section, where $i = 1, 2$ identifies, respectively, the left and right sub-FBGs separated by the phase shift. Its elements are given by [21]

$${}^{i}F_{11} = {}^{i}F_{22}^{*} = \cosh(\gamma L_i) - j\left(\frac{\widehat{\sigma}}{\gamma}\right) \cdot \sinh(\gamma L_i) \tag{3}$$

$${}^{i}F_{12} = {}^{i}F_{21}^{*} = -j\left(\frac{\kappa}{\gamma}\right) \cdot \sinh(\gamma L_i) \tag{4}$$

where * denotes complex conjugation, L_i is the corresponding sub-grating length (see Fig. 1), $\gamma^2 = \kappa^2 - \widehat{\sigma}^2$, κ is the "ac" coupling coefficient defined as $\kappa = \omega \cdot \Delta n/(2c)$ and Δn is the refractive index change, $\widehat{\sigma}$ is the general "dc" self-coupling coefficient defined as $\widehat{\sigma} = n_{\mathrm{eff}} \cdot (\omega - \omega_D)/c$, n_{eff} is the effective refractive index, c is the velocity of light in vacuum, ω is the angular frequency of the incident light wave, and ω_D is the angular frequency corresponding to the Bragg wavelength of the sub-FBGs.

Based on the coupled-mode theory and the transmission-matrix approach [21], the amplitude reflection coefficient $\rho(\omega)$, the power reflection coefficient $r(\omega)$, and the phase response $\theta(\omega)$ of the PS-FBG can be expressed, respectively, as

$$\rho(\omega) = \frac{\dfrac{{}^{1}F_{11}}{{}^{1}F_{21}} - \left(\dfrac{{}^{2}F_{11}}{{}^{2}F_{21}}\right)^{*} \cdot \exp(j\varphi_{\mathrm{PS}})}{\dfrac{{}^{1}F_{11} \cdot {}^{2}F_{11}}{({}^{1}F_{21} \cdot {}^{1}F_{21}) - \exp(j\varphi_{\mathrm{PS}})}} \tag{5}$$

$$r(\omega) = |\rho(\omega)|^2 \tag{6}$$

$$\theta(\omega) = \mathrm{phase}[\rho(\omega)]. \tag{7}$$

After reflection at the PS-FBG, the modified electrical field $E_{\mathrm{IM}}(t)$ of the phase-modulated light wave can then be expressed as

$$\begin{aligned} E_{\mathrm{IM}}(t) &= \sqrt{r(\omega_o)}E_o J_0(\beta)\exp[j\omega_o t + j\theta(\omega_o)] \\ &\quad + \sqrt{r(\omega_o+\omega_e)}E_o J_1(\beta) \\ &\quad \times \exp\left\{j\left(\omega_o t + \omega_e t + \varphi_e + \frac{\pi}{2}\right) + j\theta(\omega_o+\omega_e)\right\} \\ &\quad - \sqrt{r(\omega_o-\omega_e)}E_o J_1(\beta) \\ &\quad \times \exp\left\{j\left(\omega_o t - \omega_e t - \varphi_e - \frac{\pi}{2}\right) + j\theta(\omega_o-\omega_e)\right\}. \end{aligned} \tag{8}$$

Due to the PM–IM conversion, we could have an intensity-modulated signal at the output of the PD. The recovered microwave signal $V(\omega_e)$ and its power $P(\omega_e)$ are given by

$$\begin{aligned} V(\omega_e) &\propto \mathrm{ac}\left\{|E_{\mathrm{IM}}(t)|^2\right\} \\ &\approx A \times \left\{\sqrt{r(\omega_o+\omega_e)} \cdot \cos(\omega_e t + \theta_1)\right. \\ &\quad \left. - \sqrt{r(\omega_o-\omega_e)} \cdot \cos(\omega_e t + \theta_2)\right\} \end{aligned} \tag{9}$$

$$\begin{aligned} P(\omega_e) &\propto |V(\omega_e)|^2 \\ &\approx A^2 \cdot \left\{r(\omega_o+\omega_e) + r(\omega_o-\omega_e)\right. \\ &\quad \left. - 2\sqrt{r(\omega_o+\omega_e)\,r(\omega_o-\omega_e)} \cdot \cos(\theta_1-\theta_2)\right\} \end{aligned} \tag{10}$$

where

$$A = 2{E_o}^2 J_0(\beta) J_1(\beta)\sqrt{r(\omega_o)} \tag{11}$$

$$\theta_1 = \varphi_e + \frac{\pi}{2} + \theta(\omega_o+\omega_e) - \theta(\omega_o) \tag{12}$$

$$\theta_2 = \varphi_e + \frac{\pi}{2} + \theta(\omega_o) - \theta(\omega_o-\omega_e) \tag{13}$$

and $\mathrm{ac}(\cdot)$ denotes the ac term of the output electrical signal. If no first-order sidebands fall in the notch or the phase jump, we have

$$\sqrt{r(\omega_o+\omega_e)} = \sqrt{r(\omega_o-\omega_e)} \tag{14}$$

$$\theta_1 - \theta_2 = \theta(\omega_o+\omega_e) + \theta(\omega_o-\omega_e) - 2\theta(\omega_o) = 0 \tag{15}$$

which are obtained assuming the top of the reflection spectrum is flat and the phase response within the reflection spectrum, except the phase jump, is linear. Substituting (14) and (15) into (10), we have $P(\omega_e) = 0$. This explains that the detection of a phase-modulated signal at a PD would generate no microwave signals, except a dc. If one sideband falls in the notch of the PS-FBG, neither (14), nor (15) is satisfied and we have $P(\omega_e) > 0$, which indicates that the phase-modulated signal is converted to an intensity-modulated signal and the detection of the intensity-modulated signal at a PD will generate a microwave signal. Therefore, due to PM–IM conversion at the PS-FBG, a narrow passband corresponding to the ultra-narrow notch in the reflection spectrum of the PS-FBG is resulted, an MPF with a narrow passband is thus realized.

The frequency response of the MPF can be calculated using (9) after incorporating $r(\omega)$ and $\theta(\omega)$ of the PS-FBG. Since L_i, which indicates the position where the phase shift is introduced, and the phase shift φ_{PS} are two important parameters in $r(\omega)$ and $\theta(\omega)$, we calculate the $r(\omega)$, $\theta(\omega)$, and $P(\omega_e)$ for different values of L_i and φ_{PS}.

Fig. 3(a) and (b) shows the theoretically calculated $r(\omega)$ and $\theta(\omega)$ for φ_{PS} at three different values, 0.9π, π, and 1.1π, where $L_1 = L_2$. The total length of the PS-FBG is 10 mm with an n_{eff} of 1.45 and a Δn of 4×10^{-4}. Fig. 3(c) shows the corresponding frequency responses $P(\omega_e)$. From Fig. 3, we can see when φ_{PS} is π, a notch is observed at the center of the reflection spectrum with a phase jump corresponding to a single phase cycle. We assume here that the optical carrier frequency is larger than the notch frequency. The center frequency of the passband of the

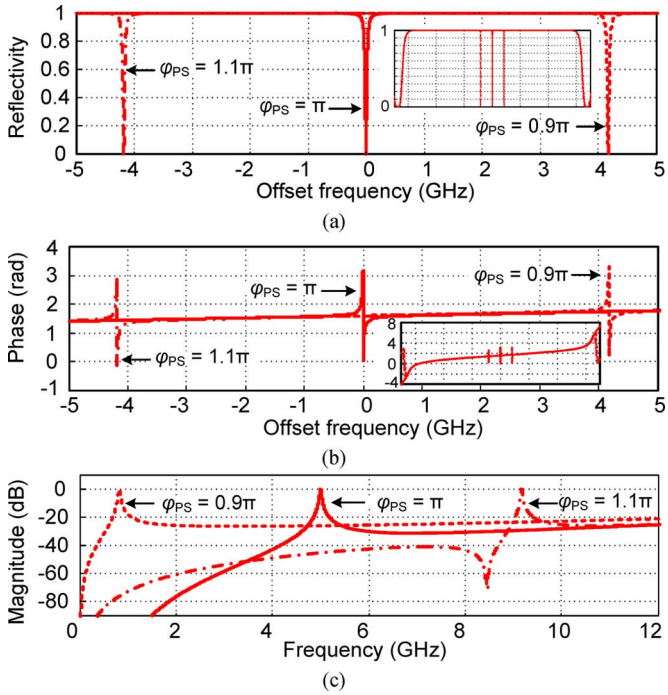

Fig. 3. PS-FBG with different phase shifts of 0.9π, π, and 1.1π. (a) Theoretical reflection spectra of the PS-FBG. (b) Theoretical phase responses of the PS-FBG (The insets in (a) and (b) show the corresponding reflection spectra and phase responses with a much larger frequency span of 70 GHz.) (c) Theoretical frequency responses of the MPF for different phase shifts.

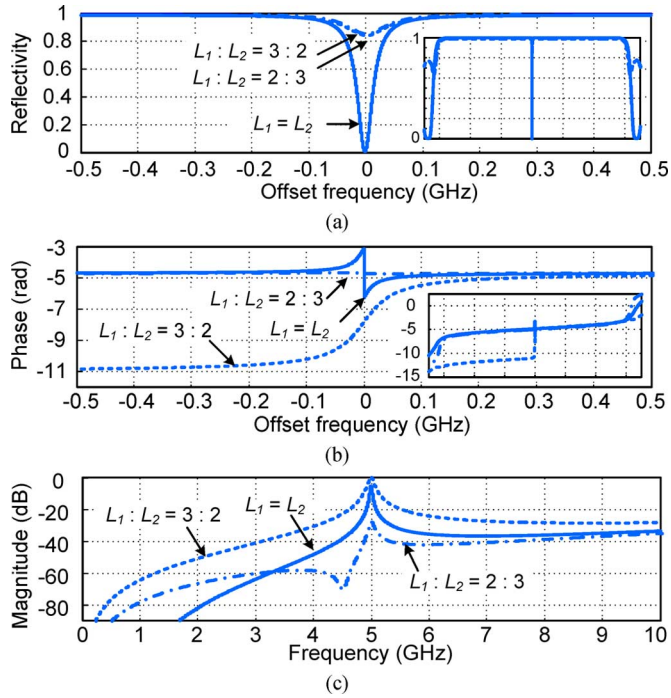

Fig. 4. Impact of the length difference between L_1 and L_2 on the reflection magnitude and phase responses of the PS-FBG. (a) Theoretical reflection spectra of the PS-FBG. (b) Theoretical phase responses of the PS-FBG; (The insets in (a) and (b) show the corresponding reflection spectra and phase responses with a much larger frequency span of 70 GHz.) (c) Theoretical frequency response of the obtained MPF.

MPF is equal to the frequency difference between the optical carrier frequency and the center frequency of the notch. If $\varphi_{\rm PS}$ is greater or smaller than π, the center frequency of the notch is shifted to a smaller or a greater frequency, and the center frequency of the passband of the MPF is also accordingly increased or decreased. Therefore, we can see that the phase shift $\varphi_{\rm PS}$ only determines the location of the notch and the phase jump within the notch, and would further determine the center frequency of the MPF for a given optical carrier frequency.

The length difference between L_1 and L_2 will have an impact on the notch and the phase jump of the PS-FBG, and thus the passband of the MPF. Fig. 4(a) and (b) shows the theoretically calculated $r(\omega)$ and $\theta(\omega)$ for $L_1 = L_2$, $L_1 < L_2$, and $L_1 > L_2$, given $\varphi_{\rm PS}$ is equal to π. As can be seen for $L_1 = L_2$, the PS-FBG has the deepest notch with a single phase cycle corresponding to the notch, and the 3-dB bandwidth of the passband of the corresponding MPF, as shown in Fig. 4(c), is the smallest, which is equal to the 3-dB bandwidth of the notch. If $L_1 < L_2$, (say, $L_1 : L_2 = 2 : 3$), both the notch depth and the phase jump become smaller. The small notch depth and phase jump would lead to an inefficient PM–IM conversion, thus a very weak passband in the MPF frequency response would be observed. If L_1 is larger than L_2 (say, $L_1 : L_2 = 3 : 2$), despite that the notch depth becomes smaller, a fast 2π-phase jump corresponding to the notch is generated. Due to the fast and large phase jump, an efficient PM–IM conversion is obtained, leading to a strong passband in the MPF response. However, since the frequency range corresponding to the 2π-phase jump is wider than that for $L_1 = L_2$ where the phase response has a single phase cycle, the 3-dB bandwidth of the passband is also increased, which leads to a smaller Q factor of the MPF.

Therefore, to obtain a high-Q MPF, it is preferable to employ a symmetric PS-FBG where $L_1 = L_2$ to ensure a narrow notch with a fast phase jump. Since the notch and the phase jump can be controlled as narrow as a few megahertz [19] and the width of the MPF passband is equal to that of the notch, the bandwidth of the MPF can be as narrow as a few megahertz, leading to a high-Q value. For example, if the 3-dB bandwidth of the notch of the symmetric PS-FBG is 10 MHz, the 3-dB bandwidth of the MPF would also be 10 MHz; assuming the center frequency of the MPF is 10 GHz, a Q factor as large as 1000 is thus obtained. The key significance of the proposed MPF is that a large tunable range can be achieved by simply tuning the wavelength of the optical carrier while maintaining a narrow and fixed passband. In addition, the passband can be potentially designed to have a shape with flat top and sharp transitions by designing the magnitude and phase response of the PS-FBG.

III. Experiment and Discussion

An experiment based on the setup shown in Fig. 1 is performed. A VNA is employed to measure the frequency response of the MPF. A microwave sinusoidal signal from the VNA is applied to the phase modulator with a frequency (ω_e) sweeping from 50 MHz to 10 GHz. The power of the signal is fixed at 5 dBm. The half-wave voltage of the phase modulator is 15 V. The phase modulation index is about 0.12 so that small-signal modulation is guaranteed. The key device in the proposed MPF is the PS-FBG, which is fabricated using a uniform phase mask by scanning an UV beam along the axial direction of an optical fiber. A π phase shift is introduced at the center of the grating by shifting the phase mask by half the corrugation width to create

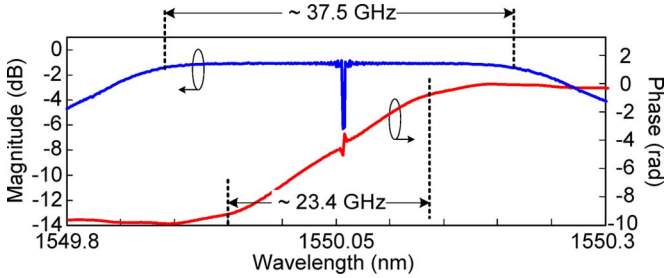

Fig. 5. Measured reflection magnitude and phase responses of the PS-FBG.

an ultra-narrow notch at the middle of the reflection spectrum. The phase response in the notch has a phase jump corresponding to a single phase cycle. The reflection magnitude and phase responses of the PS-FBG are measured using an optical vector analyzer, and are shown in Fig. 5. There is an ultra-narrow notch at about 1550.055 nm in the middle of the reflection spectrum and a single phase cycle in the phase response. The total reflection bandwidth of the PS-FBG is about 37.5 GHz, but the bandwidth in which the phase response is linear is about 23.4 GHz. The 3-dB bandwidth of the notch is about 120 MHz

The PS-FBG is then incorporated into the proposed MPF to perform PM–IM conversion. The wavelength of the optical carrier is set at a wavelength that is less than the center wavelength of the notch; the upper sideband will fall in the notch of the PS-FBG when the microwave frequency is equal to the frequency difference between the frequency of the optical carrier and the center frequency of the notch. To measure the spectral response of the MPF, a microwave sinusoidal signal generated by the VNA with a sweeping frequency from 50 MHz to 10 GHz is applied to the phase modulator. The output signal from the PS-FBG is then applied to the PD. The tuning of the center frequency of the MPF is achieved by changing the wavelength of the optical carrier. Fig. 6(a) shows the superimposed frequency responses of the MPF with the central frequency tuned from about 1 GHz to about 6.5 GHz with a tuning step of about 700 MHz. The frequency tuning range here is about 5.5 GHz, which is limited by the reflection bandwidth of the PS-FBG. The tuning range could be further increased to tens of gigahertz by using a PS-FBG with a wider reflection bandwidth. The frequency tuning resolution is limited by the smallest wavelength tuning step of the TLS.

From Fig. 6(a), we can also see that the insertion loss of the MPF is more than 30 dB. Such a high insertion loss is mainly caused by the poor optical power handling capability of the PD. By using a high-power handling PD [22], [23], the insertion loss can be greatly reduced. The ratio of the transmission peak to the sidelobe can be as large as 25 dB. When tuning the center frequency of the passband, the ratio would be smaller. The degradation in peak to the sidelobe ratio is resulted from the amplitude and phase response ripples of the PS-FBG. The PM–IM conversion at the PS-FBG would convert the ripples to noise. In addition, given a certain modulation frequency, as the wavelength of the optical carrier is shifting away from the notch, one sideband of the phase-modulated light wave would be falling outside the reflection spectrum, PM–IM conversion would also happen, and another passband starting at such a frequency would appear, as

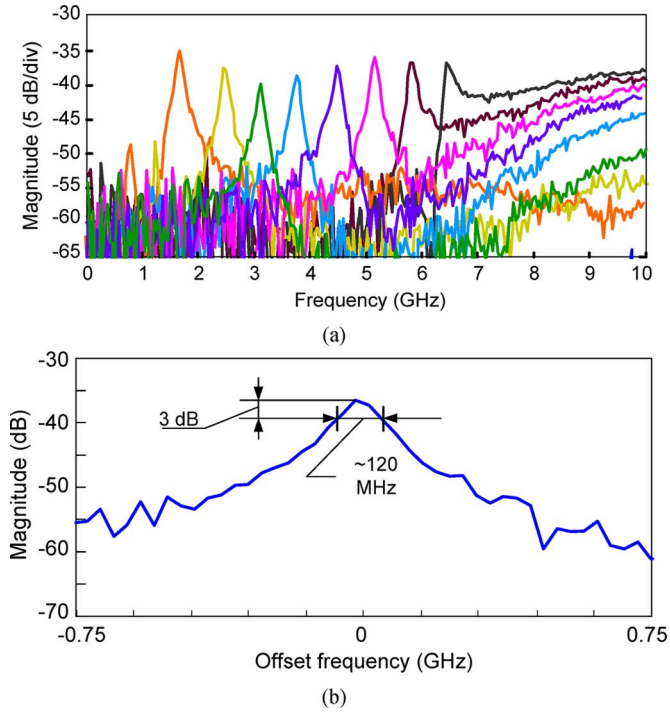

Fig. 6. (a) Measured frequency responses of the MPF with the central frequency tuned from about 1 GHz to about 6.5 GHz with a tuning step of about 700 MHz. (b) Zoom-in view of the frequency response when the center frequency is tuned at about 4.9 GHz.

shown in Fig. 6(a). A solution to avoid the second passband is to use a PS-FBG with a wider reflection bandwidth.

The average 3-dB bandwidth of the MPF is about 135 MHz; the variation of the 3-dB bandwidth over the tuning range is about 15 MHz. Such a variation is also caused by the magnitude and phase response ripples of the PS-FBG.

Fig. 6(b) shows a zoom-in view of the measured frequency response of the MPF with a center frequency of 4.9 GHz. The 3-dB bandwidth is about 120 MHz, which is equal to the 3-dB bandwidth of the notch of the PS-FBG. The bandwidth of the MPF can be further reduced by using a PS-FBG with a narrower notch and a narrower phase jump within the notch.

Theoretically, the central frequency of the MPF can be as close to zero as the optical carrier is close to the notch. Thus, the frequency tunability range of the proposed MPF is from zero to the largest central frequency of the MPF. As the optical carrier is shifting away from the notch, the central frequency of the MPF and the lower cutoff frequency of the second passband are increasing and decreasing, respectively, and would be finally identical when the frequency spacing between the optical carrier and the notch is identical to the frequency spacing between the optical carrier and the closer edge of the reflection spectrum. Therefore, the largest central frequency is equal to the minimum lower cutoff frequency, and the frequency tunability range here is from zero to the largest central frequency.

For a given PS-FBG, assume that the total reflection bandwidth of the PS-FBG is B, and the reflection bandwidths of two sub-gratings are xB and $(1-x)\,B$. The value of x would be less than or equal to 0.5. The optical carrier is assumed to locate in the reflection band with a reflection bandwidth of $(1-x)\,B$ (see

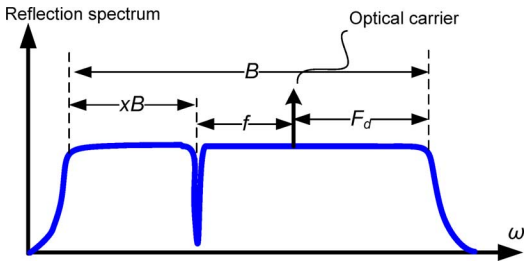

Fig. 7. Illustration of the parameters of the PS-FBG for the calculation of the frequency tunable range of the MPF.

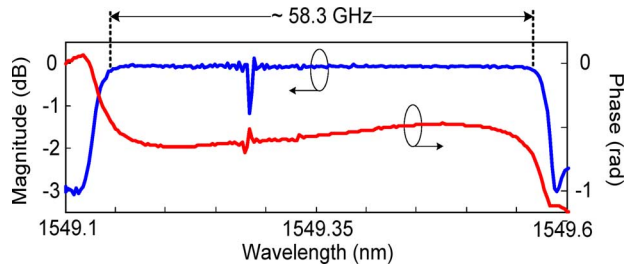

Fig. 8. Measured reflection magnitude and phase response of the second PS-FBG.

Fig. 7). Thus, the lower cutoff frequency F_d, which is the frequency spacing between the optical carrier and the closer edge of the reflection spectrum, can be expressed as

$$F_d = \min\left[xB + f, (1-x)B - f\right] = \begin{cases} xB + f, & 0 \le f \le \dfrac{(1-2x)B}{2} \\ (1-x)B - f, & \dfrac{(1-2x)B}{2} \le f \end{cases} \tag{16}$$

where f is the frequency difference between the frequency of the optical carrier and that of the notch, and also is the center frequency of the MPF. Considering the condition that the central frequency f should be less than the lower cutoff frequency F_d, we have $f < (1-x)B - f$. We can then have the upper limit of f for (16), given by $f < [(1-x)B]/2$.

Since the frequency tunable range of the MPF is the minimum lower cutoff frequency, it can be expressed as F_T

$$F_T = \min(F_d) = \min\left(xB, \frac{(1-x)B}{2}\right) = \begin{cases} xB, & 0 \le x \le \dfrac{1}{3} \\ \dfrac{(1-x)B}{2}, & \dfrac{1}{3} < x \le \dfrac{1}{2}. \end{cases} \tag{17}$$

From (17), we can see that the frequency tunable range is a function of both the reflection bandwidth and the location of the notch, namely, the value of x. For the PS-FBG employed in the experiment, the notch is located at the middle of the reflection spectrum, which means x is equal to 1/2. The tuning range F_T should be equal to one-fourth of the reflection bandwidth, i.e., $37.5/4 \approx 9.4$ GHz. However, the reflection bandwidth with a linear phase response is only about 23.4 GHz, in which the notch is not located at the middle, and the value of x is equal to about 0.42, as can be seen in Fig. 5. Therefore, a second passband would appear at a frequency smaller than 9.4 GHz, which is about $23.4 \times (1-0.42)/2 = 7.02$ GHz. In Fig. 6(a), we can see that a second passband with a lower cutoff frequency of around 7 GHz exists, which limits the tunable range to be within 7 GHz.

Although the tuning range can be increased by using a PS-FBG with a wider reflection bandwidth, the maximum tuning range of the MPF for a given reflection bandwidth of B would be achieved when x is equal to 1/3, which is $B/3$. Based on (5), the value of x can be optimized by choosing a proper value of φ_{PS} in the design.

A second experiment is then performed in which the first PS-FBG is replaced by a second PS-FBG with a wider reflection bandwidth and a narrower notch. The location of the notch is adjusted by adjusting the phase shift such that the value of x is 1/3. Thus, a maximum tuning range is obtained. The measured magnitude and phase responses of the new PS-FBG are shown in Fig. 8. As can be seen, the location of the notch is at 1549.275 nm, corresponding to an x of 1/3. The reflection bandwidth is about 0.46 nm or 58.5 GHz. Therefore, the tuning range could be as large as 19.5 GHz.

The wavelength of the optical carrier is set at 1549.275 nm, which is more than the center wavelength of the notch; therefore the lower sideband will fall in the notch of the PS-FBG when the microwave frequency is equal to the difference between the frequency of the optical carrier and the center frequency of the notch. By increasing the wavelength of the optical carrier, the center frequency of the MPF is accordingly increased. Fig. 9(a) shows the superimposed frequency responses of the MPF with a tunable central frequency covering a frequency range of about 15 GHz with a tuning step of 1.45 GHz. From Fig. 9(a), we can also see that the ratio of the transmission peak to the sidelobe can be as large as 40 dB. The frequency tuning range here is less than the theoretical result of 19.5 GHz, which is caused by the limited bandwith of the 10-GHz PD. The second passband is not seen since it is eliminated by the PD due to its limited bandwidth. The central frequency dependency of the frequency response of the MPF is resulted from the frequency-dependent response of the 10-GHz PD. At the high frequency band ($>$ 10 GHz), the electrical frequency response of the PD becomes small, which leads to the power reduction of the recovered microwave signal. In Fig. 9(b), a zoom-in view of the measured frequency response of one MPF at about 6.9 GHz is shown. The 3-dB bandwidth is about 60 MHz. The bandwidth can be further decreased by using a PS-FBG with a narrower notch.

The average 3-dB bandwidth of the second MPF is about 72 MHz. The variation of the 3-dB bandwidth over the tuning range is about 15 MHz, as shown in Fig. 10. Such a variation is also caused by the nonlinearity of the phase response of the PS-FBG, which leads to the frequency-dependency of PM–IM conversion.

Another important performance measure for the MPF is the dynamic range (DR). In the earlier analysis, small-signal modulation is considered. For small-signal modulation, only the optical carrier and the first-order sidebands are considered. However, as the power of the input signal or equivalently the phase

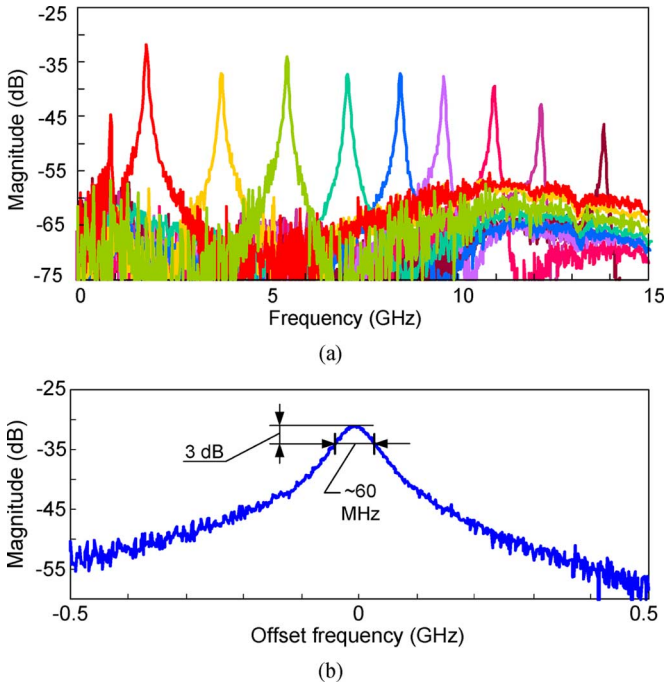

Fig. 9. (a) Measured frequency responses of the MPF when a second PS-FBG is employed. (b) Zoom-in view of the frequency response when the center frequency is tuned at 6.9 GHz.

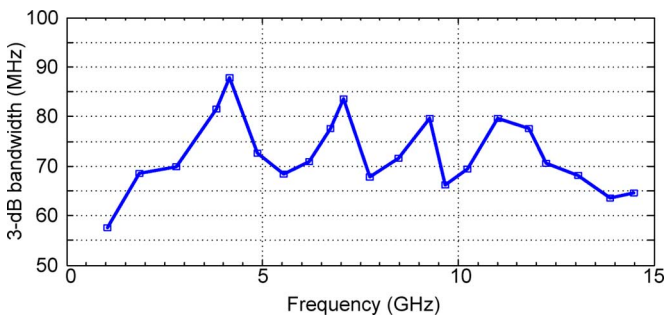

Fig. 10. Relationship between the 3-dB bandwidth of the MPF and the central frequency.

modulation index increases, the power of the higher order sidebands would increase, thus nonlinear distortions start.

The DR here is defined as the range from the minimum discernable signal (lower limit) to the maximum allowable signal (upper limit). The lower limit is directly measured here by the VNA, which is −37 dBm. The upper limit determined by the nonlinearity of the phase modulator is quantified by the 1-dB compression point. Namely, in the analysis, the upper limit is found when the transmission peak of the frequency response of the MPF drops by 1 dB from the maximum value.

For convenience and simplicity, we assume the reflectivity of the PS-FBG is one and the notch of the PS-FBG is deep enough to totally suppress the +first-order sideband of the phase-modulated light wave. The optical carrier and the other sidebands are totally reflected by the PS-FBG. Therefore, the power of the recovered microwave signal can be expressed as the summation of the power of the beatings between any adjacent sidebands.

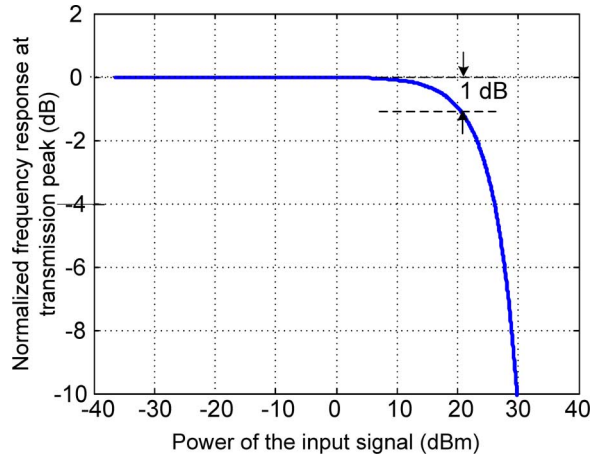

Fig. 11. Frequency response at the transmission peak versus the power of the input signal ($V\pi = 10$ V).

Based on (1), the electrical field $E_{\mathrm{IM}}{}'(t)$ at the input of the PD can be expressed as

$$\begin{aligned} &E_{\mathrm{IM}}{}'(t) \\ &\quad\approx E_o \sum_{n=2}^{\infty} i^n J_n(\beta) \exp\{j[\omega_o t + n(\omega_e t + \varphi_e)]\} \\ &\qquad + E_o \sum_{n=-\infty}^{0} i^n J_n(\beta) \exp\{j[\omega_o t + n(\omega_e t + \varphi_e)]\} \\ &\quad= E_o \sum_{n=2}^{\infty} i^n J_n(\beta) \exp\{j[\omega_o t + n(\omega_e t + \varphi_e)]\} \\ &\qquad + E_o \sum_{n=0}^{\infty} i^n J_n(\beta) \exp\{j[\omega_o t - n(\omega_e t + \varphi_e)]\}. \end{aligned} \quad (18)$$

From (18), if only consider the fundamental frequency, we can see that: 1) the fundamental frequency generated by beating the optical carrier and the −first-order sideband is in phase with a beat signal between any two adjacent lower sidebands. All these beat signals are grouped in group A; 2) the beat signals between any two adjacent upper sidebands are in phase. All these beat signals are grouped in group B; 3) the two groups of beat signals are out of phase. Therefore, the power of the recovered microwave signal can be expressed as

$$\begin{aligned} P'(\omega_e) &\propto \left| \sum_{n=0}^{\infty} J_n(\beta) J_{n+1}(\beta) - \sum_{n=2}^{\infty} J_n(\beta) J_{n+1}(\beta) \right|^2 \\ &= \left| \sum_{n=0}^{1} J_n(\beta) J_{n+1}(\beta) \right|^2. \end{aligned} \quad (19)$$

Based on (19), the level at the transmission peak of the frequency response of the MPF as a function of the power of the input signal is shown in Fig. 11. From Fig. 11, we can see that the input power corresponding to the 1-dB compression point is about 20 dBm. Since the minimum measurable output power is −37 dBm, the 1-dB compression DR of the proposed MPF is 57 dB. When the power of the input signal increases, more and more power of the incident light wave will be distributed to

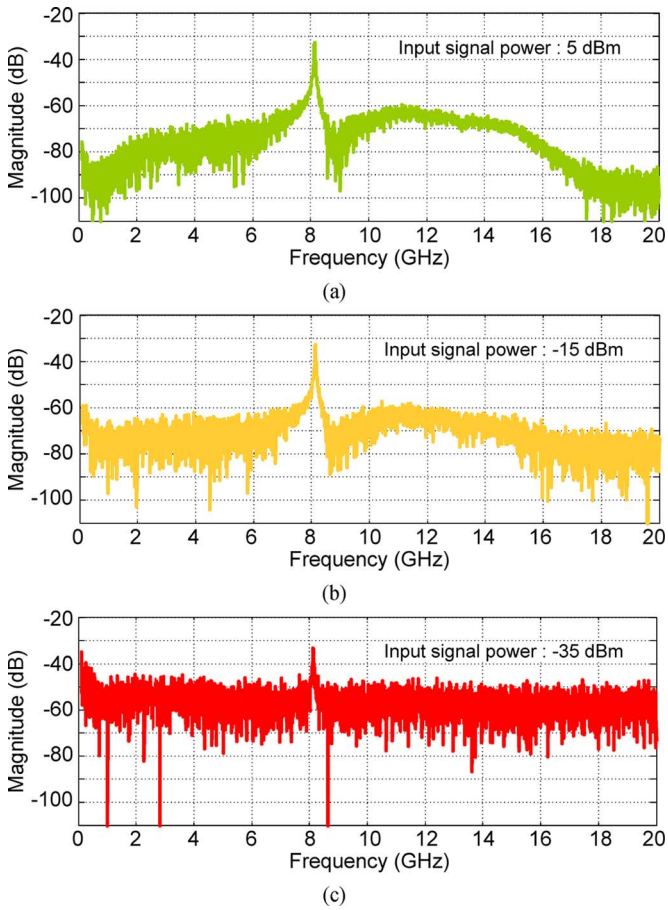

Fig. 12. Frequency response of the MPF using the second PS-FBG at different input signal power levels. (a) 5 dBm. (b) −15 dBm. (c) −35 dBm.

high-order sidebands, which leads to the power reduction of the recovered signal and the fast decrease of the frequency response of the MPF at the transmission peak.

Due to the fact that the frequency response of the MPF is determined by the PS-FBG, the change of the power of the input signal within the DR would not distort the profile of the transmission band of the MPF. Fig. 12 shows the frequency responses of the MPF using the second PS-FBG at different input signal power levels.

From Fig. 12, we can see that as the power of the input signal decreases, the profile of the transmission band of the MPF barely distorted. Thus, as the power of the input signal decreases, we

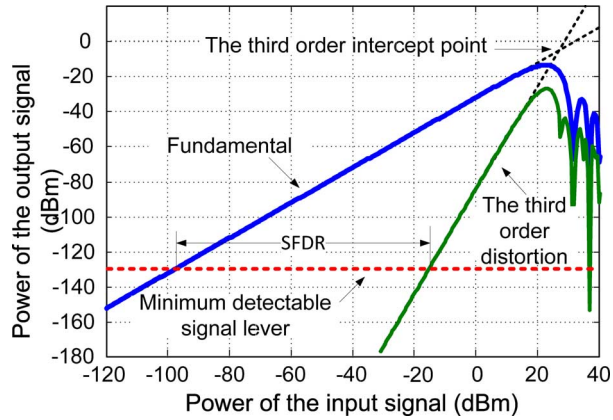

Fig. 13. Powers of the fundamental signal and the third-order intermodulation terms as a function of the input power of the input signal ($V\pi = 10$ V).

can see that the power of the recovered signal decreases and the ratio of the transmission peak to the sidelobe also decreases.

The DR can also be characterized by the spurious-free dynamic range (SFDR). Assume that two closely spaced microwave signals, $V\cos(\omega_{e1}t+\varphi_{e1})$ and $V\cos(\omega_{e2}t+\varphi_{e2})$, are applied to the input of the MPF, where ω_{e1} and ω_{e2} are angular frequencies, φ_{e1} and φ_{e2} are the initial phases of the two microwave signals, and the two signals have identical amplitudes. The electrical field $E_{\mathrm{PM}}{}'(t)$ at the output of the phase modulator can be expressed as (20), shown at the bottom of this page, where the high-order sidebands ($|n+m|\geq 4$) are ignored due to their relatively low power levels when the phase modulation index is small.

Assume that PS-FBG is used to suppress the +first-order sideband of the phase-modulated light wave, which is $\omega_o+\omega_{e1}$. After heterodyning at the PD, two third-order intermodulation terms would occur at $2\omega_{e1}-\omega_{e2}$ and $2\omega_{e2}-\omega_{e1}$. In the following, we will calculate the power of the third-order intermodulation term at $2\omega_{e1}-\omega_{e2}$.

To simplify the calculation, we consider the nature of the phase modulation: a phase-modulated signal will not generate any microwave signal, except a dc if directly detected at a PD. Based on this property, if the sideband at $\omega_o+\omega_{e1}$ is not removed by the PS-FBG, the third-order intermodulation term at $2\omega_{e1}-\omega_{e2}$ generated by beating the sidebands at $\omega_o+\omega_{e1}$ and $\omega_o-\omega_{e1}+\omega_{e2}$ would have an equal amplitude, but opposite phase with that generated by beating all other sidebands. Thus, the power of the third-order intermodulation term at $2\omega_{e1}-\omega_{e2}$

$$
\begin{aligned}
E_{\mathrm{PM}}{}'(t) &= E_o\exp\{j[\omega_o t+\beta(\cos(\omega_{e1}t+\varphi_{e1})+\cos(\omega_{e2}t+\varphi_{e2}))]\} \\
&= E_o\exp(j\omega_o t)\sum_{n=-\infty}^{\infty}\sum_{m=-\infty}^{\infty}\{i^{n+m}J_n(\beta)J_m(\beta)\exp[jn(\omega_{e1}t+\varphi_{e1})+jm(\omega_{e2}t+\varphi_{e2})]\} \\
&\approx E_o\exp(j\omega_o t)\sum_{n=-2}^{2}\sum_{m=-1}^{1}\{i^{n+m}\cdot J_n(\beta)J_m(\beta)\exp[jn(\omega_{e1}t+\varphi_{e1})+jm(\omega_{e2}t+\varphi_{e2})]\} \qquad (20)
\end{aligned}
$$

when the PS-FBG is used to remove $\omega_o + \omega_{e1}$ can be obtained by calculating the power of the term generated by only beating the sidebands $\omega_o + \omega_{e1}$ and $\omega_o - \omega_{e1} + \omega_{e2}$. Thus, the power of the third-order intermodulation term at $2\omega_{e1} - \omega_{e2}$ can be expressed as

$$P''(2\omega_{e1} - \omega_{e2}) \propto \left| i \cdot J_1(\beta) J_0(\beta) \cdot i^{-1} i J_{-1}(\beta) J_1(\beta) \right|^2 = \left| J_0(\beta) J_1^3(\beta) \right|^2. \quad (21)$$

Based on (19) and (21), we can plot the output powers of the fundamental and the third-order intermodulation terms as a function of the input power, as shown in Fig. 13. The third-order intercept point is about 26 dBm. Considering the minimum detectable signal level in the proposed system, which is decided by the noise floor, is -130 dBm/Hz, the SFDR is about 81 dB $\cdot$ Hz$^{2/3}$.

IV. Conclusion

A simple and novel approach to implementing a narrow-passband and frequency-tunable MPF based on PM–IM conversion employing a phase modulator and a PS-FBG was proposed and experimentally demonstrated. A theoretical analysis was performed in which the value of the phase shift and the location of the phase shift in the PS-FBG on the frequency response of the MPF were studied. Two PS-FBGs with different reflection bandwidths and phase-shift values introduced at the center of the gratings were fabricated and incorporated into the proposed MPF. For the two PS-FBGs, the 3-dB bandwidths of the MPF were 120 and 60 MHz and the tunable ranges were 5.5 and 15 GHz. Both the width of the passband and the tunable range could be further improved by using a PS-FBG with a narrower notch and a wider reflection bandwidth. The key advantage of the proposed technique is that the MPF can be tuned with a large tunable range up to tens of gigahertz and high tuning speed, which is difficult for a purely electronic microwave filter. In addition, the notch profile can be controlled, which enables the design and implementation of an MPF with a specific frequency response, such as a passband with a flat top and sharp transitions. However, due to the low power handling capability of the PD, the insertion loss of the MPF is large. A solution is to use a high power-handling PD.

Acknowledgment

The authors gratefully acknowledge TeraXion Inc., Quebec City, QC, Canada, for providing the PS-FBGs used in the experiment.

References

[1] J. Capmany and D. Novak, "Microwave photonics combines two worlds," *Nat. Photon.*, vol. 1, no. 6, pp. 319–330, Jun. 2007.

[2] J. Yao, "Microwave photonics," *J. Lightw. Technol.*, vol. 27, no. 3, pp. 314–335, Feb. 2009.

[3] C. K. Madsen and J. H. Zhao, *Optical Filter Design and Analysis, A Signal Processing Approach*. New York: Wiley, 1999.

[4] J. Capmany, B. Ortega, and D. Pastor, "A tutorial on microwave photonic filters," *J. Lightw. Technol.*, vol. 24, no. 1, pp. 201–229, Jan. 2006.

[5] B. Vidal, T. Mengual, C. Ibanez-Lopez, and J. Marti, "WDM photonic microwave filter with variable cosine windowing based on a DGD module," *IEEE Photon. Technol. Lett.*, vol. 18, no. 21, pp. 2272–2274, Nov. 2006.

[6] D. Pastor, B. Ortega, J. Capmany, S. Sales, A. Martinez, and P. Muñoz, "Optical microwave filter based on spectral slicing by use of arrayed waveguide gratings," *Opt. Lett.*, vol. 28, no. 19, pp. 1802–1804, Oct. 2003.

[7] J. Mora, B. Ortega, A. Díez, J. L. Cruz, M. V. Andrés, J. Capmany, and D. Pastor, "Photonic microwave tunable single-bandpass filter based on a Mach–Zehnder interferometer," *J. Lightw. Technol.*, vol. 24, no. 7, pp. 2500–2509, Jul. 2006.

[8] K. Zhu, H. Ou, H. Fu, E. Remb, and S. He, "A simple and tunable single-bandpass microwave photonic filter of adjustable shape," *IEEE Photon. Technol. Lett.*, vol. 20, no. 23, pp. 1917–1919, Dec. 2008.

[9] E. Hamidi, D. E. Leaird, and A. M. Weiner, "Tunable programmable microwave photonic filters based on an optical frequency comb," *IEEE Trans. Microw. Theory Tech.*, vol. 58, no. 11, pp. 3269–3278, Nov. 2010.

[10] N. You and R. A. Minasian, "A novel high-Q optical microwave processor using hybrid delay-line filters," *IEEE Trans. Microw. Theory Tech.*, vol. 47, no. 7, pp. 1304–1308, Jul. 1999.

[11] J. Capmany, "On the cascade of incoherent discrete-time microwave photonic filters," *J. Lightw. Technol.*, vol. 24, no. 7, pp. 2564–2578, Jul. 2006.

[12] B. Ortega, J. Mora, J. Capmany, D. Pastor, and R. Garcia-Olcina, "Highly selective microwave photonic filters based on active optical recirculating cavity and tuned modulator hybrid structure," *Electron. Lett.*, vol. 41, no. 20, pp. 1133–1135, Sep. 2005.

[13] E. Xu, X. Zhang, L. Zhou, Y. Zhang, Y. Yu, X. Li, and D. Huang, "Ultrahigh-Q microwave photonic filter with Vernier effect and wavelength conversion in a cascaded pair of active loops," *Opt. Lett.*, vol. 35, no. 8, pp. 1242–1244, Apr. 2010.

[14] B. Vidal, M. A. Piqueras, and J. Martí, "Tunable and reconfigurable photonic microwave filter based on stimulated Brillouin scattering," *Opt. Lett.*, vol. 32, no. 1, pp. 23–24, Jan. 2007.

[15] S. Chin, L. Thevenaz, J. Sancho, S. Sales, J. Capmany, P. Berger, J. Bourderionnet, and D. Dolfi, "Broadband true time delay for microwave signal processing, using slow light based on stimulated Brillouin scattering in optical fibers," *Opt. Exp.*, vol. 18, no. 21, pp. 22599–22613, Oct. 2010.

[16] X. Yi and R. A. Minasian, "Microwave photonic filter with single bandpass response," *Electron. Lett.*, vol. 45, no. 7, pp. 362–363, Mar. 2009.

[17] J. Palací, G. E. Villanueva, J. V. Galán, J. Martí, and B. Vidal, "Single bandpass photonic microwave filter based on a notch ring resonator," *IEEE Photon. Technol. Lett.*, vol. 22, no. 17, pp. 1276–1278, Sep. 2010.

[18] F. Zeng and J. P. Yao, "Investigation of phase modulator based all-optical bandpass microwave filter," *J. Lightw. Technol.*, vol. 23, no. 4, pp. 1721–1728, Apr. 2005.

[19] Y. Painchaud, M. Aubé, G. Brochu, and M. Picard, "Ultra-narrowband notch filtering with highly resonant fiber Bragg gratings," in *Bragg Gratings, Photosensitivity, and Poling in Glass Waveguides, OSA Tech. Dig.*, 2010, Art. ID BTuC3, [CD ROM].

[20] G. Qi, J. P. Yao, J. Seregelyi, C. Bélisle, and S. Paquet, "Optical generation and distribution of continuously tunable millimeter-wave signals using an optical phase modulator," *J. Lightw. Technol.*, vol. 23, no. 9, pp. 2687–2695, Sep. 2005.

[21] T. Erdogan, "Fiber grating spectra," *J. Lightw. Technol.*, vol. 15, no. 8, pp. 277–1294, Aug. 1997.

[22] A. Ramaswamy, M. Piels, N. Nunoya, T. Yin, and J. E. Bowers, "High power silicon-germanium photodiodes for microwave photonic applications," *IEEE Trans. Microw. Theory Tech.*, vol. 58, no. 11, pp. 3336–3343, Nov. 2010.

[23] C. L. Goldsmith, G. A. Magel, B. M. Kanack, and R. J. Baca, "Coherent combining of RF signals in a traveling-wave photodetector array," *IEEE Photon. Technol. Lett.*, vol. 9, no. 7, pp. 988–990, Jul. 1997.

Wangzhe Li (S'08) received the B.Eng degree in electronic science and technology from Xi'an Jiaotong University, Xi'an, China, in 2004, the M.Sc degree in optoelectronics and electronic science from Tsinghua University, Beijing, China, in 2007, and is currently working toward the Ph.D. degree in electrical

engineering at the School of Electrical Engineering and Computer Science, University of Ottawa, Ottawa, ON, Canada.

His current research interests include photonic generation of microwave and terahretz signals.

Ming Li (S'08–M'09) received the Ph.D. degree in electrical and electronics engineering from the University of Shizuoka, Hamamatsu, Japan, in 2009.

In April 2009, he joined the Microwave Photonics Research Laboratory, School of Electrical Engineering and Computer Science, University of Ottawa, Ottawa, ON, Canada, as a Postdoctoral Research Fellow. His current research interests include advanced FBGs and their applications to microwave photonics, ultrafast optical signal processing, arbitrary waveform generation, and optical microelectromechanical systems (MEMS) sensing.

Jianping Yao (M'99–SM'01–F'12) received the Ph.D. degree in electrical engineering from the Université de Toulon, Toulon, France, in 1997.

In 2001, he joined the School of Electrical Engineering and Computer Science, University of Ottawa, Ottawa, ON, Canada, as an Assistant Professor. In 2003, he became an Associate Professor, a Full Professor in 2006, and in 2007, he became the University Research Chair. From July 2007 to June 2010, he was the Director of the Ottawa–Carleton Institute for Electrical and Computer Engineering. Prior to joining the University of Ottawa, from 1999 to 2011, he was an Assistant Professor with the School of Electrical and Electronic Engineering, Nanyang Technological University, Singapore. He has authored or coauthored over 360 papers, including over 200 papers in peer-reviewed journals and 160 papers in conference proceedings. He is an Associate Editor for the *International Journal of Microwave and Optical Technology*. His research has focused on microwave photonics, which includes photonic processing of microwave signals, photonic generation of microwave, millimeter wave and terahertz, radio-over-fiber, ultra-wideband (UWB) over fiber, and photonic generation of microwave arbitrary waveforms. His research also covers fiber optics and bio-photonics, which includes fiber lasers, fiber and waveguide Bragg gratings, fiber-optic sensors, microfliudics, optical coherence tomography, and Fourier-transform spectroscopy. He has been a a Principal Investigator on over 20 projects, including five strategic grant projects funded by the Natural Sciences and Engineering Research Council of Canada (NSERC).

Dr. Yao is a Registered Professional Engineer of the Province of Ontario. He is a Fellow of the Optical Society of America (OSA). He is a Fellow of the IEEE Microwave Theory and Techniques Society (IEEE MTT-S) and the IEEE Photonics Society. He is on the Editorial Board of the IEEE TRANSACTIONS ON MICROWAVE THEORY AND TECHNIQUES. He is a chair of numerous international conferences, symposia, and workshops, including vice Technical Program Committee (TPC) chair of the 2007 IEEE Microwave Photonics Conference, TPC co-chair of the 2009 and 2010 Asia–Pacific Microwave Photonics Conference, TPC chair of the High-Speed and Broadband Wireless Technologies Subcommittee of the 2009, 2010, 2011, and 2012 IEEE Radio Wireless Symposium, TPC chair of the Microwave Photonics Subcommittee of the 2009 IEEE Photonics Society Annual Meeting, TPC chair of the 2010 IEEE Microwave Photonics Conference, and general co-chair of 2011 IEEE Microwave Photonics Conference. He is also a committee member of numerous international conferences. He was the recipient of the 2005 International Creative Research Award of the University of Ottawa and the 2007 George S. Glinski Award for Excellence in Research. He was a recipient of a 2008 NSERC Discovery Accelerator Supplements Award.